Photocatalytically-driven H_2 production over Cu/TiO_2 catalysts decorated with multi-walled carbon nanotubes

Javier Fernández-Catalá[1], Miriam Navlani-García[1], Priyanka Verma[2], Ángel Berenguer-Murcia[1], Kohsuke Mori[2,3], Yasutaka Kuwahara[2,3], Hiromi Yamashita[2,3*], Diego Cazorla-Amorós[1]

[1]*Materials Institute and Inorganic Chemistry Department, University of Alicante, Ap. 99, E-03080 Alicante, Spain.*

[2]*Division of Materials and Manufacturing Science, Graduate School of Engineering, Osaka University, 2-1 Yamada-oka, Suita, Osaka 565-0871, Japan*

[3]*Unit of Elements Strategy Initiative for Catalysts & Batteries (ESICB), Kyoto University, Katsura, Kyoto 615-8520, Japan*

**Corresponding author: yamashita@mat.eng.osaka-u.ac.jp*

Abstract

In this study, we assessed the effect of the incorporation of multi-walled carbon nanotubes (MWCNT) on a TiO_2 support containing different active metals to obtain Metal/TiO_2-MWCNT photocatalytic systems. The materials prepared in this work were characterized by ICP-OES, TEM, EDX, XRD, PL, UV-Vis, and nitrogen physisorption techniques. Among those investigated metals, Cu was shown to be the most promising for the present application. The assessment of the photocatalytic performance of Cu/TiO_2-MWCNT with various Cu contents revealed that the catalytic activity depends on the Cu loading and the photocatalyst with 1 wt.% of Cu displayed the best performance among investigated. The incorporation of MWCNT in the support enhanced the photocatalytic activity towards the production of H_2 under visible and UV-Visible light irradiation at room temperature.

Keywords: *TiO_2, MWCNT, transition metal nanoparticles, H_2 production and visible-light-enhanced activity, ammonia borane decomposition.*

1. Introduction

Due to the limited resources and serious environmental problems associated to Carbon economy, one of the important challenges for the scientific community is changing the current energy scenario towards sustainable alternatives. In this sense, Hydrogen (H_2) is nowadays recognized as a candidate for a renewable and clean energy economy because it has high energy density and clean burning [1]. However, important limitations related to the safe storage, handling and distribution of H_2 are still under consideration [2]. An interesting alternative to solve these problems is the use of hydrogen carrier molecules, such as formic acid or ammonia borane (AB) [3-6].

In the last years, the scientific community has payed attention to the production of H_2 from AB due to its interesting properties such as high hydrogen content (19.6 wt. %), high gravimetric and volumetric densities (196 $gH_2\ kg^{-1}$ and 146 $gH_2\ L^{-1}$, respectively), low molecular weight (30.87 $g\ mol^{-1}$), high stability and low toxicity [7-9], etc.

Numerous studies have already been reported by investigating the performance of noble-metal based catalysts with various compositions (Au, Ru, Pt, Rh and Pd) [10-15]. Such catalysts usually show interesting results under mild conditions, but they have drawbacks related to the scarcity and high price of noble metals. With this problem in mind, the scientific community is focused on designing catalysts based on transition metals, such as Cu, Ni, Co and Fe, among others, both in the form of monometallic or bimetallic nanoparticles combined with noble metals [16,17]. As for the support, a wide variety of materials has already been studied (carbon materials, oxides, zeolites, or metal organic frameworks (MOFs)), with the purpose of minimizing the load of metal used, stabilizing the nanoparticles and improving the catalytic activity of the nanoparticles [18-24].

Another interesting alternative considered in the literature is the photocatalytically-driven AB decomposition [13,14]. However, despite the importance of titanium dioxide (TiO_2) in photocatalysis, the role of TiO_2-based catalysts as photoactive material in this application has not been widely investigated so far due to its inherent deficiencies in terms of high band gap energy which could only be excited by UV light ($\lambda < 380$ nm) and high recombination rate of electron–hole pairs. An interesting alternative to improve the properties of TiO_2 as photocatalyst and support is the incorporation of carbon materials to form TiO_2/carbon systems [25,26]. In this sense, the use of multi-walled carbon nanotubes (MWCNT) has attracted a great interest in the last decades due to their interesting properties, such as high electrical conductivity, high electron storage capacity and high-surface area (typically between 200-400 m^2/g) [27-30]. The beneficial effect of incorporating carbon nanotubes to photocatalytic systems has been widely reported in the literature. Usually, such composites are combined with noble metal nanoparticles such as Au and Pt [31-34], while transition metals-based photocatalysts with carbon material/TiO_2 composites have been less explored so far. Within them, Cu-based photocatalysts deserve special attention. In this sense, Nourbakhsh et al. developed a photocatalyst based on a mesoporous TiO_2 combined with CNT/Cu nanocomposites, which showed enhanced activity in the photodegradation of methyl orange with increasing copper content [35]. Dasireddy et al. reported an interesting heterogenous catalyst based on CNT-supported Cu and TiO_2 for the selective photocatalytic oxidation of benzene to phenol [36]. Shafei et al. synthesized a Cu-doped TiO_2-CNT catalyst, which showed a lower recombination rate as compared to pure TiO_2, and displayed better activity in the degradation of methylene blue under visible light irradiation than TiO_2-CNT or pure TiO_2 [37].

With this in mind, in this work TiO_2-MWCNTs composites were prepared as support of transition metal photocatalysts for their use towards the production of H_2 from AB decomposition. Among the different transition metals investigated (Cu, Ni and Co), Cu-based systems showed the best activity under the experimental conditions used. The role of the carbon material was also herein assessed.

2. Materials and methods

2.1 Materials

Titanium (IV) butoxide (TTB, 97%, Sigma-Aldrich), Multi-walled Carbon Nanotubes (MWCNT, Nanoblack, bamboo-type MWCNT with a diameter between 15 and 30 nm), glacial acetic acid (HAc, 99%, Sigma-Aldrich), Pluronic F-127 (F-127, Sigma-Aldrich), absolute ethanol (EtOH, 99.8%, Fisher Scientific), formamide (FA, 99.5%, Sigma-Aldrich), urea (99%, Merck), sodium borohydride ($NaBH_4$, 98%, Sigma-Aldrich), copper nitrate ($Cu(NO_3)_2 \cdot 3H_2O$, 99%, Nacalai Tesque), nickel nitrate ($Ni(NO_3)_2 \cdot 6H_2O$, 99.99%, Sigma-Aldrich), cobalt nitrate ($Co(NO_3)_2 \cdot 6H_2O$, 98%, Sigma-Aldrich), ammonia borane (AB, $H_3N \cdot BH_3$, 97%, Sigma-Aldrich), commercial TiO_2 (P25, Rutile:Anatase / 85:15, 99.9%, Degussa) and deionized water were used in the present work. All reactants were used as received, without further purification.

2.2 Catalyst preparation

2.2.1 Synthesis of supports (TiO_2 and TiO_2-MWCNT composites).

TiO_2 support was prepared using a synthetic protocol described previously by our research group [38]. For the synthesis of the TiO_2, 5 g of the titanium precursor (TTB) were dissolved in 7.9 g of EtOH. This solution (labelled “Solution A”) was stirred vigorously for 10 min. Then, 1.6 g of HAc, 0.3 g of F-127, 1.6 g of H_2O, 7.9 g EtOH, 0.4 g of FA, and 0.4 g of urea were added in another vessel (labelled “Solution B”). The

mixture was stirred for 10 min. “Solution B” was added dropwise to “Solution A” under vigorous stirring. The obtained solution was quickly transferred to an autoclave and heated at 60 ℃ for 24 h to promote the gel formation and the temperature was then increased to 120 ℃ for 24 h with the objective of promoting the decomposition of urea. The solid obtained was calcined at 350 ºC with the purpose of removing the template. For the TiO_2/MWCNT composites, we have adapted the synthesis of TiO_2 incorporating the needed amount of MWCNTs (1 wt. %) in “Solution B”. The MWCNTs were then dispersed in “Solution B” with an ultrasound probe (Bandelin SONOPULS HD 2200) with a power of 660 W operating at 30 % power for 5 min. After this step, the synthesis was performed under the same conditions described for the support based on bare TiO_2. The supports obtained in this work were named as TiO_2 and TiO_2-MWCNT, respectively.

2.2.2. Preparation of transition metal (Cu, Co, and Ni) based photocatalysts.

Photocatalysts based on as-synthesized TiO_2 and TiO_2-MWCNT, as well as on commercial P25 were prepared by following a standard impregnation protocol followed by a reduction step with $NaBH_4$. For that, 500 mg of support (TiO_2, TiO_2-MWCNT or P25) were suspended in 10 mL of deionized water and stirred for 1 h. After that, the necessary amount of a solution of the metal precursor was added so as to have a final metal loading of 1 wt.% and the mixture was stirred for 1 h at room temperature. Then, the metal ions were reduced by incorporation of a freshly prepared $NaBH_4$ aqueous solution (molar ratio between metal and $NaBH_4$ was 1:10) and the solution was stirred for 1 h. Finally, the mixtures were centrifuged (5000 rpm) to collect the catalysts and they were quickly washed with a mixture of water and ethanol (1:1 in volume) three times in order to totally remove the $NaBH_4$ present in the samples. The washed catalysts were kept under vacuum to prevent the oxidation by air. In the case of Cu-containing samples, additional photocatalysts with different Cu loadings (1, 2, and 5 wt.%) were obtained by

the same procedure. The obtained photocatalysts were denoted as (CuX%/TiO_2-MWCNT).

2.2.3 Characterization of the support and photocatalysts

Thermogravimetric analysis was performed in a TA SDT 2960 thermobalance, in which the samples were heated up at 900 °C in air (heating rate of 10 °C min^{-1}). X-ray diffraction (XRD) at room temperature was performed using a Miniflex II Rigaku equipment (30 kV/15 mA) with Cu Kα radiation and a scanning rate of 2º/min, in the 2θ range 6-80º. Nitrogen adsorption-desorption isotherms at -196 ºC were performed in an Autosorb-6B apparatus from Quantachrome Corporation. Prior to the analysis, samples were degassed at 250 °C for 4 h under vacuum. BET surface area (S_{BET}) and total micropore volume (V_{DR}) were determined by applying the Brunauer-Emmett-Teller (BET) equation, and the Dubinin-Raduskevich equation to the N_2 adsorption data obtained at -196 °C, respectively. Total pore volumes (V_t) were determined from the adsorbed nitrogen volume at a relative pressure of 0.95. X-ray Photoelectron Spectroscopy (XPS) was performed using a K-α spectrometer from Thermo-Scientific, equipped with an Al anode. Transmission electron microscopy (TEM) images were recorded using a JEOL JEM-2010 equipment. The metal loading was determined by inductively coupled plasma-optical emission spectroscopy (ICP-OES) with a Perkin-Elmer Optima 4300 system. UV-Vis diffuse reflectance spectra were collected in a Shimadzu UV-2600 spectrophotometer. $BaSO_4$ was used as background, and the absorption spectra were obtained using the Kubelka-Munk function. Photoluminescence measurements at room temperature were taken on a Fluorolog-3 spectrofluorometer (HORIBA). The excitation wavelength used for the photoluminescence analysis was 380 nm.

2.3 Catalytic tests

The performance of the prepared photocatalysts towards the production of H_2 from AB dehydrogenation reaction was evaluated as follows: 20 mg of photocatalyst was suspended in 5 mL of deionized water in a sealed test tube (66 mL) and the system was purged with argon gas in the suspension for 30 min under stirring. Then, a solution of AB (500 μL, 0.04 M) was introduced in the mixture under stirring. The activity of the materials was assessed under dark, UV-Visible light irradiation or visible light irradiation conditions ($\lambda > 420$ nm). The photocatalytic tests were performed by using a 500 W Xenon lamp (San-Ei Electric Co. Ltd.XEF-501S). The photoreactor was cooled by a fan in order to maintain a constant temperature (26 ± 0.5 ºC) during the photocatalytic reaction.

The H_2 evolution profiles were obtained by analyzing the evolved gas with an Agilent 6890A gas chromatograph equipped with a MS-5A column and a TCD detector. The reusability of the catalysts was evaluated by performing three consecutive runs. For that, the solvent was removed by centrifugation and the spent catalyst was placed in the reactor, purged with argon gas, and a fresh AB solution was injected. The reaction was monitored under the same experimental conditions as those used in the first reaction run.

3. Results and Discussion

3.1 Support Characterization

Table 1 includes the results of the characterization of the support materials. The content of MWCNTs in the TiO_2-MWCNT support was determined by thermogravimetric analysis. The carbon content was calculated to be around 1 wt. %, which was in good agreement with the nominal MWCNTs loading. With respect to the crystallite size obtained by XRD analysis of the supports, TiO_2 and TiO_2-MWCNT have the characteristic peaks of the anatase phase and smaller crystallite TiO_2 size with respect to

the commercial P25 [38]. Moreover, the incorporation of MWCNT in the synthesis leads to a slight increase of the TiO_2 crystallite size in the composite support. The N_2 adsorption-desorption isotherms are shown in Fig. S1. The N_2 physisorption isotherm of commercial P25 shows a type-II isotherm, characteristic of a nonporous solid. As-synthesized TiO_2 and TiO_2-MWCNT showed a combination of type I and IV isotherms, which is typical of mesoporous materials with a certain degree of microporosity. However, TiO_2-MWCNT has a more developed mesoporosity because it presents an increase in the hysteresis and an increase of the V_t value as shown in Table 1. As for the textural properties, the results obtained from the adsorption-desorption experiments revealed that BET surface area and V_t for the as-synthesized TiO_2 and TiO_2-MWCNT are higher as compared to the commercial P25 [38].

Table 1. MWCNT content (wt. %), crystallite size of TiO_2 and textural properties of the supports.

Support	MWCNT (wt. %)[a]	TiO_2 crystal size (nm)[b]	Surface area (m^2/g)	V_t (cm^3/g)	V_{DR} (cm^3/g)
P25	-	25	50	0.05	0.01
TiO_2	-	7.6	170	0.35	0.06
TiO_2-MWCNT	1.06	9.1	176	0.46	0.07

[a] Determined from the weight loss in the interval of 450-680 ºC
[b] Determined from the Scherrer's equation

TEM images are presented in Fig. S2. The supports TiO_2 and TiO_2-MWCNT have a smaller size of TiO_2 particles with respect to the commercial P25. Moreover, it is possible to observe the presence of MWCNT in the sample TiO_2-MWCNT and the good contact between both components of the composite.

3.2 Study of the effect of MWCNT in the Metal/TiO_2-MWCNT system

The evaluation of the composition of the catalysts was initiated with the study of the performance of various transition-metal-based photocatalysts supported on TiO_2-MWCNT for H_2 generation from AB dehydrogenation under visible light irradiation conditions. The metal content was ~ 1 wt.% in all cases (See Table S1). The comparison of the H_2 evolution profiles achieved with Cu, Ni, and Co photocatalysts is plotted in Figure S3. As it can be seen, Co-based photocatalysts displayed a very poor performance, producing 1.8 µmol after 35 min of reaction. In the case of Ni-based photocatalysts, a long reaction time was needed to achieve a total conversion of AB to H_2, while it was achieved after only 15 min for the Cu-based photocatalysts, revealing the superior performance of Cu1%/TiO_2-MWCNT over the Ni and Co counterpart samples. Such observation might be related to the more favored reduction of copper species under reaction conditions and the subsequent generation of metal active sites as compared to other composition of the catalysts [19].

The effect of MWCNTs in the final materials was also analyzed by comparing the properties and photocatalytic activity of Cu1%/P25, Cu1%/TiO_2, and Cu1%/TiO_2-MWCNT. With respect to the characterization results of the photocatalyst, ICP-OES analysis shows that all photocatalysts have around 0.90 wt.% of Cu (0.87, 0.89, and 0.91 wt.%, for Cu1%/P25, Cu1%/TiO_2, and Cu1%/TiO_2-MWCNT, respectively), being the amount of copper similar to the nominal loading (1 wt.%). The XRD patterns of the Cu-containing photocatalysts are very similar to those of the Cu-free counterparts (Fig. S4). The presence of anatase in the TiO_2 and TiO_2-MWCNT supports was identified, while for the P25 support a mixture of anatase and rutile was detected [38]. No peaks ascribed to the presence of Cu (or copper oxide) species (Fig. S4) were observed, which could be due to the presence of very small Cu (or copper oxide) particles and/or the low copper

content in the samples. Such observation agrees with TEM results, in which the presence of Cu particles was not observed (Fig. S5).

Fig. 1 shows the UV-Vis absorption spectra of the supports and photocatalyst with 1 wt.% loading of Cu. TiO_2 support with the crystal phase anatase and commercial P25 with an anatase/rutile mixture (See Fig. S4), present a similar absorption edge. However, the support that contains MWCNT presents a marked increase in the absorption of visible light. Moreover, UV-Vis spectra of Cu-containing photocatalysts display an increase in the visible light absorption within the wavelength range of 600-900 nm [39]. Cu 2p XPS spectra of Cu1%/P25, Cu1%/TiO_2, and Cu1%/TiO_2-MWCNT photocatalysts are shown in Fig. S6. The Cu 2p XPS spectra usually shows the characteristic peaks of Cu^0 and Cu^+ at 932.6 and 932.18 eV, respectively, which hampers the proper assignation of these two species. However, the satellite peak of Cu^{2+} at 943 eV, makes it feasible to distinguish and analyze such species [40,41]. From the Cu 2p XPS spectra of the catalysts studied in this work, it could be extracted that Cu1%/TiO_2-MWCNT photocatalyst has only Cu^0 or Cu^+ (Fig. S6), while Cu^{2+} is detected in both Cu1%/TiO_2 and Cu1%/P25. This observation indicates that the incorporation of MWCNT in the composite material favors the existence of less oxidized Cu species (Cu^+) or stabilized Cu in zerovalent state (Cu^0).

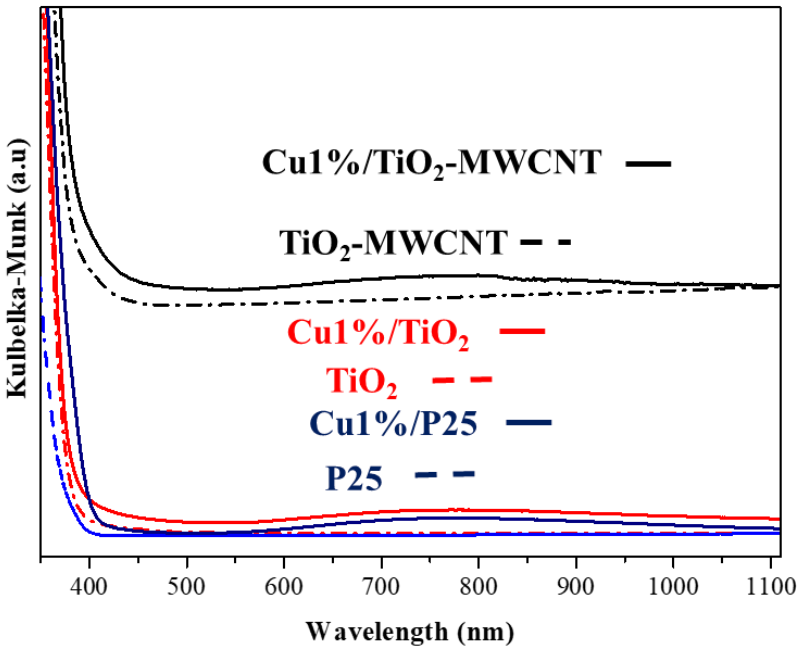

Fig. 1. UV-Vis absorption of the raw supports (P25, TiO_2, and TiO_2-MWCNT) and the photocatalyst with 1 wt. % of Cu (Cu1%/P25, Cu1%/TiO_2, and Cu1%/TiO_2-MWCNT).

Fig. 2 compares the Photoluminescence (PL) spectra of the supports (P25, TiO_2, and TiO_2-MWCNT) and the photocatalysts with 1 wt. % of Cu (Cu1%/P25, Cu1%/TiO_2, and Cu1%/TiO_2-MWCNT). The photoluminescence measurements present the spectral range from 400 to 550 nm. The band at 416 nm indicates the indirect band-to-band recombination across the band gap. The peak observed at 520 nm is assigned to the recombination of states above the valence band [42-45]. As compared to P25, PL emission intensity decreased for as-synthesized TiO_2. The incorporation of MWCNT leads to a more significant decrease of the PL emission intensity, demonstrating that the incorporation of MWCNT hampers the e^--h^+ recombination [46,47]. Moreover, it was observed that such decrease in the PL emission intensity is even more marked for Cu1%/TiO_2-MWCNT, which suggests the positive role of the presence of Cu in the resulting material.

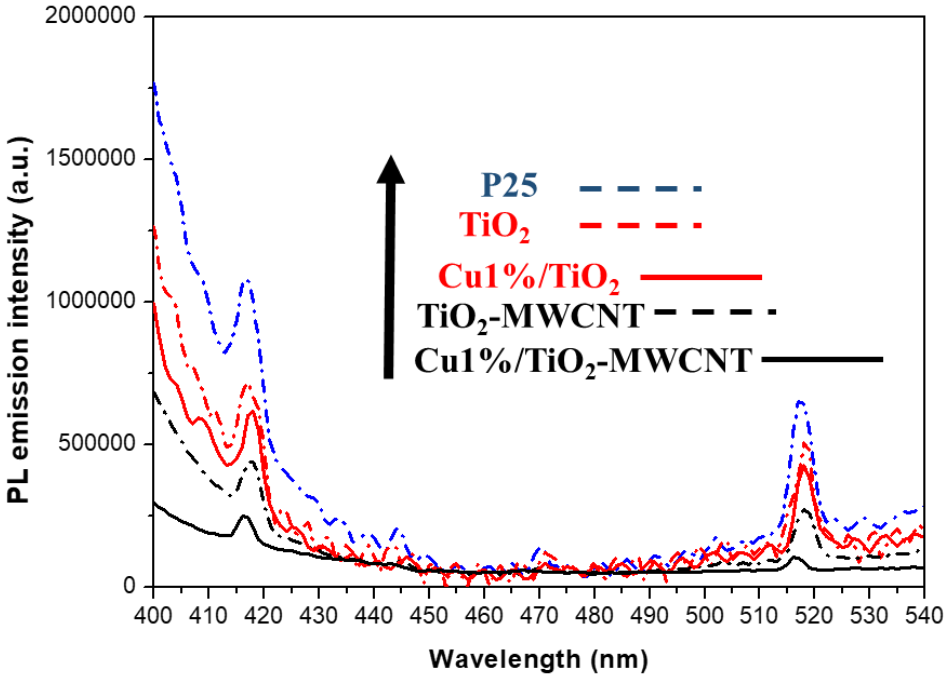

Fig. 2. Photoluminescence of P25, TiO_2, and TiO_2-MWCNT supports and Cu1%/P25, Cu1%/TiO_2, and Cu1%/TiO_2-MWCNT photocatalysts. The excitation wavelength used for the photoluminescence analysis was 380 nm.

The photocatalytic performance towards the production of H_2 from AB is displayed in Fig. 3 and Fig. S7. As it can be seen in Fig. S7, Cu-free photocatalysts showed a very poor activity, generating less than 5 μmol of H_2 after 35 min of reaction. However, Cu-containing photocatalysts showed a significant enhancement under dark conditions, visible light irradiation ($\lambda > 420$ nm) and UV-visible light at ambient temperature (Fig. S7), indicating the important role of Cu species in catalyzing the decomposition of AB [18,19,22]. Moreover, the superior performance of the materials under illumination (with both UV and UV-Vis irradiations), as expected for photoactive materials, is also evidenced in Fig. S7. The positive role of the incorporation of MWCNTs in the photocatalysts is demonstrated by comparing the results shown in Fig. S7 (b,c) and Fig. 3. As it can be observed, a better initial activity was displayed by Cu1%/TiO_2-MWCNT

as compared to the MWCNT-free counterpart. However, since such an enhancement is not only observed under irradiation conditions, but also under dark conditions (See Fig. 3), it might not be exclusively related to the photocatalytic response of the final material, but also to the intrinsic properties of the composite material.

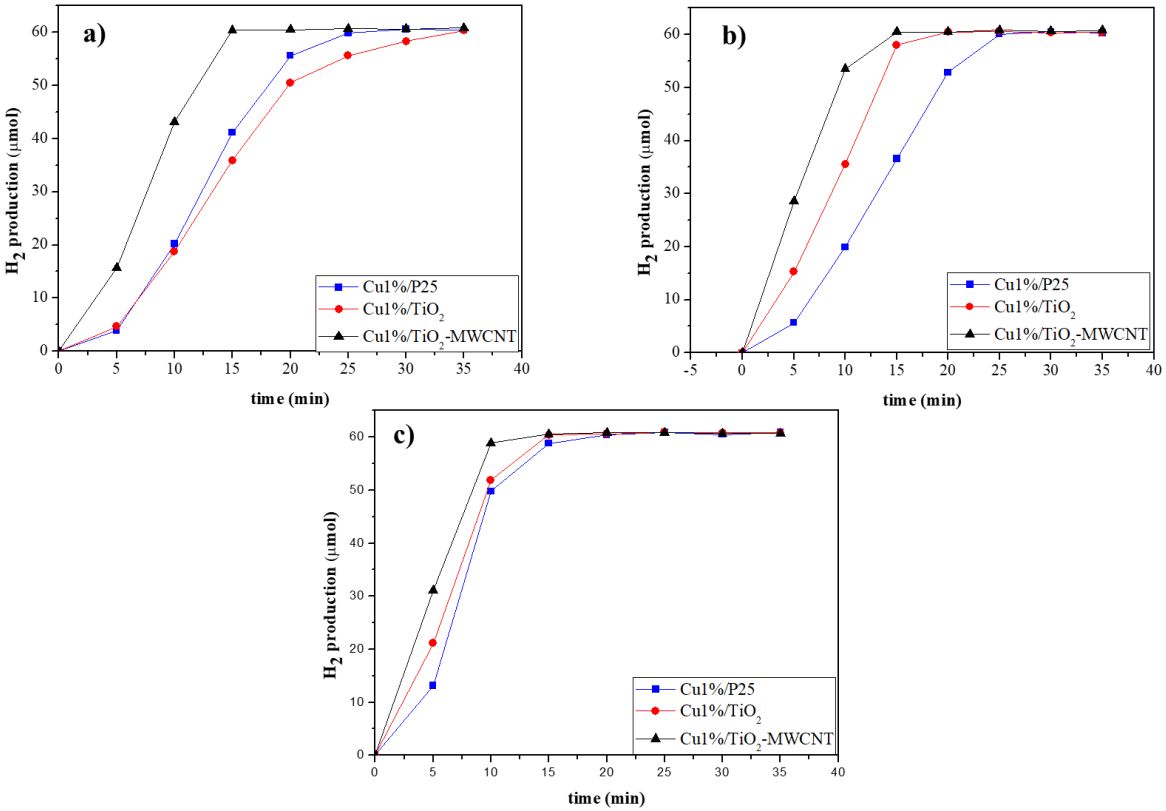

Fig. 3. H_2 generation from AB dehydrogenation over Cu1%/P25, Cu1%/TiO_2, and Cu1%/TiO_2-MWCNT photocatalysts under: a) dark conditions, b) visible light irradiation ($\lambda > 420$ nm), and c) UV-visible light irradiation at ambient temperature (~ 60 μmol H_2 represents approximately 100 % conversion of AB).

The obtained results confirmed the importance of the support in the catalytic activity of the resulting materials. It is observed that the presence of MWCNTs in the support improves the catalytic activity towards the AB dehydrogenation due to their interaction with TiO_2 resulting in the enhanced light absorption in the visible region. Moreover, the

presence of MWCNTs also reduces the e^--h^+ recombination rate, leading to a better photocatalytic performance as compared to the MWCNT-free counterpart photocatalysts.

3.3 Effect of different Cu loadings on TiO_2-MWCNT samples

The present section is focused on the optimization of the Cu content in TiO_2-MWCNT-based photocatalysts with a nominal Cu loading of 1, 2, and 5 wt.%. ICP-OES results revealed that the actual Cu content was 0.9, 1.8, and 5.2 wt.%, respectively. XRD patterns of TiO_2-MWCNT and Cu-containing photocatalysts are depicted in Fig. 4a. It can be observed that while the sample with 1 and 2 wt. % of copper showed the same diffraction patterns as the Cu-free counterpart and only the characteristic peaks of the TiO_2 anatase phase were observed, Cu5%/TiO_2-MWCNT displayed the characteristic peak of zerovalent Cu (111) at 43.2º, indicating the presence of metallic Cu. Nevertheless, it must be noted that in Fig. 4a no characteristic peaks of CuO at 36º or Cu_2O at 39º are observed. This may be because these peaks are overlapping with those of the TiO_2 anatase phase [39]. As it was previously mentioned for samples with 1 wt.% of Cu, signals related to Cu species might have not been detected in Cu1%/TiO_2-MWCNT and Cu2%/TiO_2-MWCNT due to their small size and/or the lower Cu content.

The UV-Vis absorption spectra of the photocatalysts with different Cu loading is shown in Fig. 4b. A significant increase in the absorption intensity from 600 to 900 nm (visible light) was observed due to increase in the Cu content and hence making them more sensitive to visible light [42].

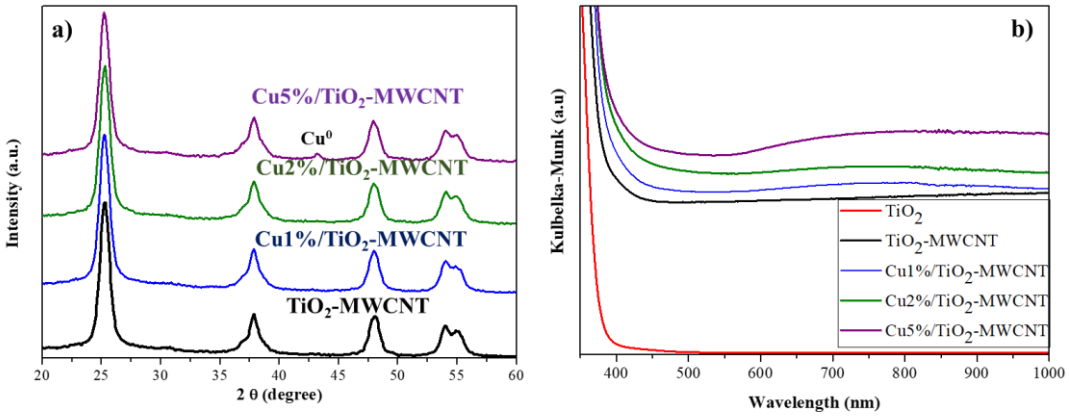

Fig. 4. Characterization of TiO_2-MWCNT support and TiO_2-MWCNT photocatalysts with different Cu loadings: a) XRD patterns, and b) UV-Vis absorption spectra.

TEM images of the photocatalysts with different Cu loadings are displayed in Fig. 5. The images show that the presence of Cu (and copper oxide) nanoparticles increased with the copper loading. In this sense, such Cu species could not be distinguished from the support matrix in Cu1%/TiO_2-MWCNT, while some agglomerates were observed in Cu2%/TiO_2-MWCNT and Cu5%/TiO_2-MWCNT photocatalysts.

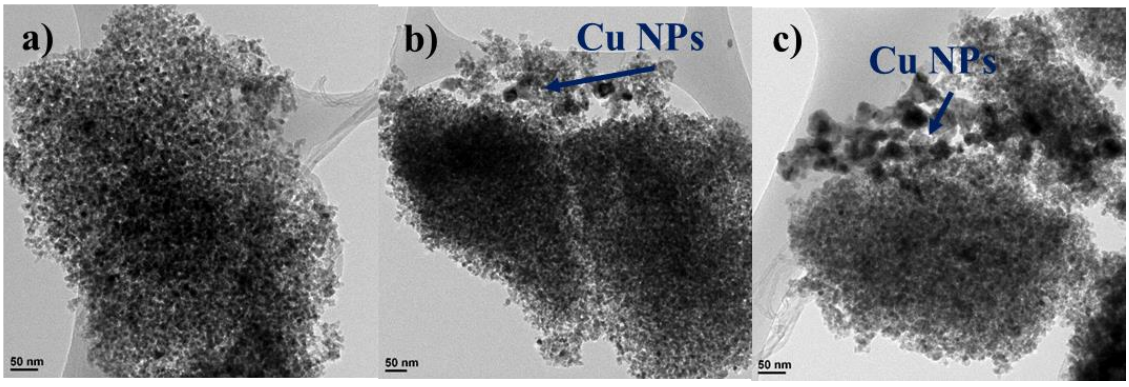

Fig. 5. TEM images of TiO_2-MWCNT-based photocatalysts with different Cu loadings: a) Cu1%/TiO_2-MWCNT, b) Cu2%/TiO_2-MWCNT, and c) Cu5%/TiO_2-MWCNT.

As it can be seen in Fig. S8, N_2 physisorption isotherms of the TiO_2-MWCNT support and photocatalysts with different Cu loadings Cu (1, 2, and 5 wt. %) show a combination of type I and IV isotherms in all cases, indicating that the Cu loading did not change the

porous texture considerably. However, a decrease in the hysteresis loop was observed in the Cu-containing photocatalysts, indicating that the Cu species are partially blocking or filling the mesopores of the support. The textural properties are listed in Table 2. As observed, photocatalysts with different Cu loadings have similar BET surface areas and total pore volumes (V_t). Nevertheless, both parameters are lower than those values obtained for the support material, confirming that Cu species are partially blocking or filling the pores of the support. Another interesting factor is that the V_{DR} does not decrease in the samples with Cu suggesting that the Cu species are not located within the micropores of the support.

Table 2. Textural properties of the TiO_2-MWCNT support and Cu-containing photocatalysts.

Sample	Surface area (m^2/g)	V_t (cm^3/g)	V_{DR} (cm^3/g)
TiO_2-MWCNT	176	0.46	0.07
Cu1%/TiO_2-MWCNT	158	0.36	0.06
Cu2%/TiO_2-MWCNT	156	0.35	0.06
Cu5%/TiO_2-MWCNT	155	0.36	0.06

The photocatalytic activity results of this series of photocatalysts (expressed as TOF values in mol H_2 · mol Cu^{-1} · min^{-1}) from AB decomposition reaction is depicted in Fig. 6. The results revealed that, as expected, the photocatalytic performance depends on the amount of Cu present in the catalyst. In this sense, the photocatalyst with the lowest amount of Cu species displayed the best photocatalytic activity (TOF values) among those investigated and an increase of Cu loading in the photocatalysts brings forth a decrease in the values of TOFs under all experimental conditions used in this study (dark, visible and UV-Vis irradiation). This effect might be ascribed to the larger size of the Cu species with increasing Cu loading in the photocatalysts (as shown in the TEM images (Fig. 5)) and the subsequent less favored contact among the components of the photocatalysts [18].

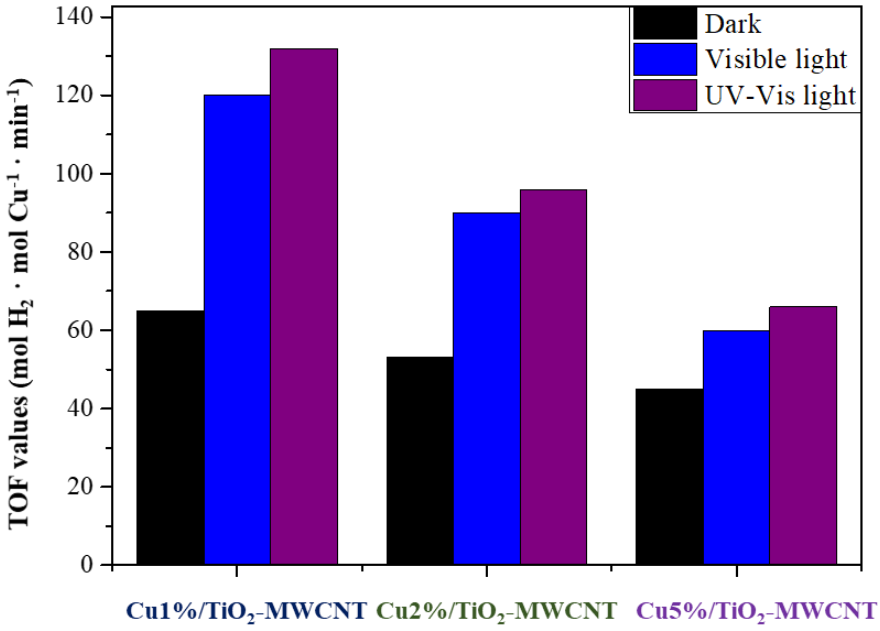

Fig. 6. TOF values of TiO_2-MWCNT photocatalysts with different Cu loadings calculated after 2.5 minutes under dark, and visible and UV-Vis irradiation conditions.

According to the results obtained in this study, an increase in the copper loading on TiO_2-MWCNT-based photocatalysts favors the formation of larger metal particles and increases the absorption of visible light without changing the textural properties of the catalyst. However, an increase in the Cu loading decreases the photocatalytic activity (TOF values) of the sample due the agglomeration of Cu species.

3.4 Evaluation of the stability of the Cu1%/TiO_2-MWCNT photocatalyst and mechanism of H_2 production from AB hydrolysis

In this section, the study is focused on the stability of the photocatalyst under investigation (Cu1%/TiO_2-MWCNT) for H_2 generation from AB dehydrogenation under visible light irradiation ($\lambda > 420$ nm).

The stability of Cu1%/TiO_2-MWCNT photocatalyst under visible light irradiation was investigated by performing three consecutive reaction cycles. After each cycle, the spent

catalyst is collected by centrifugation, placed in the reactor, and purged with argon gas. Subsequently, 500 μL of AB solution 0.04 M were injected in the reaction mixture as described in Section 2.4. Fig. 7 shows that Cu1%/TiO_2-MWCNT displayed high stability and the catalytic activity is preserved even after three consecutive reaction cycles. It should be mentioned that despite the intense investigation on the development of efficient catalysts and photocatalysts for the production of H_2 from AB, the deactivation issue is still an important limitation for some systems [18, 48, 49]. Therefore, the high stability achieved in this case makes the present photocatalytic system a promising material for the decomposition of AB.

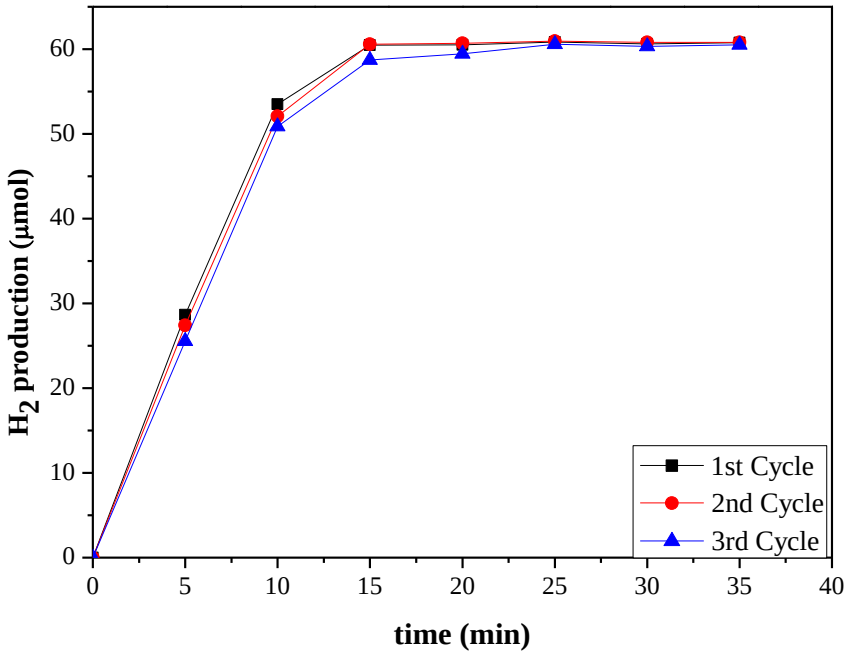

Fig. 7. Stability tests on the photocatalytic performance of Cu1%/TiO_2-MWCNT for H_2 generation from AB dehydrogenation under visible light irradiation conditions ($\lambda >$ 420 nm).

An important factor in photocatalysis is the formation of radical intermediates upon light irradiation of photoactive materials in aqueous media. For this reason, in this work the

effect of the hydroxyl radical in the photocatalytic H_2 generation from AB dehydrogenation over Cu1%/TiO_2-MWCNT under visible light irradiation was studied. To perform this analysis, 2-propanol (0.1 mL) was injected into the reaction mixture after purging with argon for 30 min to act as hydroxyl radical scavenger. Also, the effect of the superoxide anions formed by the reactions between the generated electrons and the dissolved oxygen was also assessed. For that, the photocatalyst was bubbled with oxygen gas for 10 min. Fig.8 shows the H_2 evolution profiles achieved using the experimental conditions mentioned (reactor purged with Ar gas, in presence of 2-propanol, and reactor bubbled with oxygen gas). As observed, the presence of 2-propanol (hydroxyl radical scavenger) has an effect in the performance of the photocatalysts due to the decrease of the concentration of hydroxyl radical in the reaction medium (the initial production of H_2 decreased from 28.5 to15.4 µmol of H_2 after 5 min of reaction when 2-propanol is present in the reaction medium). On the other hand, an important photocatalytic activity decay is observed when oxygen is present in the reaction medium. Such effect might be due to the oxidation of Cu and the formation of less active copper oxide species.

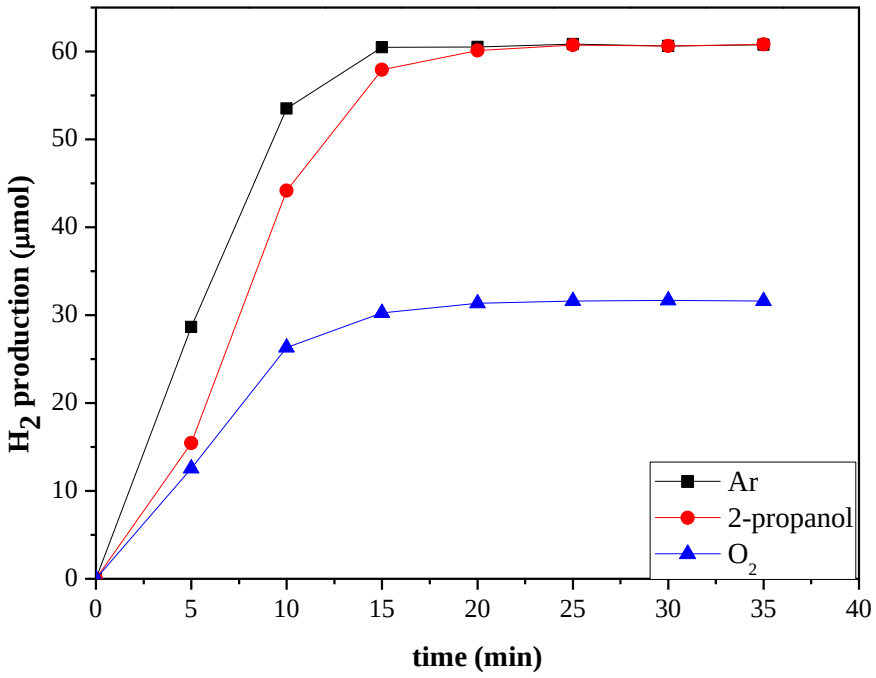

Fig. 8. Role of hydroxyl radical and superoxide anion on the photocatalytic performance of Cu1%/TiO_2-MWCNT for H_2 generation from AB dehydrogenation under visible light irradiation ($\lambda > 420$ nm).

A possible mechanism for visible-light-driven H_2 production from AB decomposition over Cu1%/TiO_2-MWCNT is proposed in Scheme 1. Upon light absorption by TiO_2 and generation of e^--h^+ pairs, holes may react with the solvent (H_2O) to form hydroxyl radicals. These radicals can react with AB molecules adsorbed on the surface of the catalyst and favor the B-N bond cleavage (pathway (a)) [19]. On the other hand, the reaction could be driven through a second pathway *via* the e- generated by the absorption of light (pathway (b)). These e^- can be transferred from the semiconductor (TiO_2) to the carbon material (acting as an electron scavenger) and then to the metal nanoparticles. This effective charge separation might enhance the electrostatic interaction between AB molecules and copper nanoparticles, favoring the dehydrogenation reaction through the interaction of the AB molecules with the solvent (water) [13]. The interesting contribution

of MWCNTs is that they can serve as electron scavenger, transferring the e^- to the Cu nanoparticles, avoiding the e^--h^+ recombination and favoring a good interaction between metal particles and AB molecules.

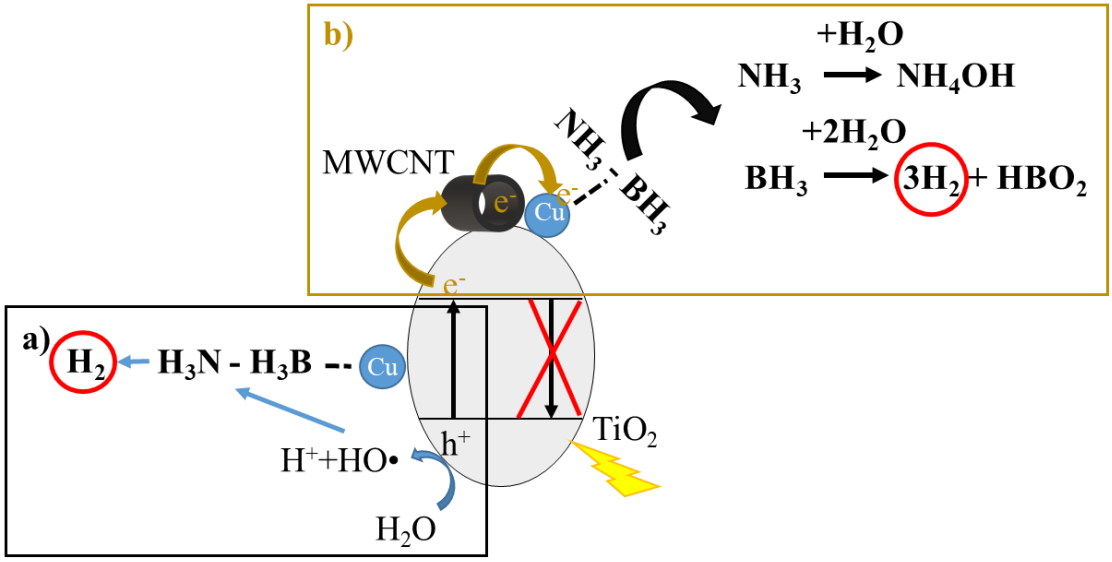

Scheme 1. Possible mechanisms for the photocatalytic enhancement of AB dehydrogenation under visible light irradiation over Cu1%/TiO_2-MWCNT photocatalysts.

4. Conclusions

In this study, TiO_2-MWCNT composites were prepared as support of transition metal photocatalysts for their use towards the production of H_2 from AB decomposition. The most relevant conclusions extracted from this work are that the support presents a great importance in the catalytic activity of the active phase (Cu nanoparticles) observing that the presence of MWCNTs improves the catalytic activity of the AB dehydrogenation under visible light irradiation probably due to the electron scavenging properties of this carbon material. It has also been observed that the catalytic activity depended on the Cu content and the sample with lower copper loading displayed better catalytic activity than those catalysts with higher copper loadings (2 and 5 wt.%). Another important factor is

that sample (Cu1%/TiO_2-MWCNT) presents high cyclability (3 cycles), which makes it a promising candidate for the present application.

Credit Author Statement

Javier Fernández-Catalá: Conceptualization, Methodology, Investigation, Writing - Original Draft and Funding acquisition. **Miriam Navlani-García**: Conceptualization, Methodology, Investigation, Writing - Original Draft, Writing - Review & Editing, Supervision. **Priyanka Verma**: Conceptualization, Investigation, Writing - Review & Editing and Supervision. **Ángel Berenguer-Murcia**: Conceptualization, Methodology, Writing - Review & Editing and Supervision. **Kohsuke Mori**: Writing - Review & Editing, Supervision. **Yasutaka Kuwahara**: Writing - Review & Editing, Supervision. **Hiromi Yamashita**: Writing - Review & Editing, Supervision, Project administration and Funding acquisition. **Diego Cazorla-Amorós**: Conceptualization, Methodology, Writing - Review & Editing, Supervision, Project administration and Funding acquisition.

Acknowledgements

The authors thank Ministerio de Ciencia Innovación y Universidades and FEDER (Project RTI2018-095291-B-I00) and the Generalitat Valenciana (PROMETEOII/2018/076) for financial support. JFC thanks MINECO for a researcher formation grant (BES-2016-078079). MNG gratefully acknowledges Generalitat Valenciana and Plan GenT (CDEIGENT/2018/027) for the postdoctoral grant. The present work was partially supported by Grants-in-Aid for Scientific Research (Nos. 26220911, 19H00838) from the Japan Society for the Promotion of Science (JSPS) and MEXT. KM, YK, and HY thank MEXT program “Elements Strategy Initiative to Form Core Research Center.

References

[1] I.P. Jain, Int. J. Hydrogen Energy. 34 (2009) 7368–7378.

[2] N. Armaroli, V. Balzani, Chem. Sus.Chem. 4 (2011) 21–36.

[3] M. Grasemann, G. Laurenczy, Energy Environ. Sci. 5 (2012) 8171–8181.

[4] M. Navlani-García, D. Salinas-Torres, D. Cazorla-Amorós, Energy 12 (2019) 4027.

[5] C.W. Hamilton, R.T. Baker, A. Staubitz, I. Manners, Chem. Soc. Rev. 38 (2009) 279–293.

[6] M. Navlani-García, K. Mori, Y. Kuwahara, H. Yamashita, NPG Asia Mater. 10 (2018) 277–292.

[7] Z. Huang, T. Autrey, Energy Environ. Sci. 5 (2012) 9257–9268.

[8] Q.L. Zhu, Q. Xu, Energy Environ. Sci. 8 (2015) 478–512.

[9] U.B. Demirci, Int. J. Hydrogen Energy. 42 (2017) 9978–10013.

[10] T. Kamegawa, T. Nakaue, Chem. Commun. 51 (2015) 16802–16805.

[11] M. Navlani-García, K. Mori, A. Nozaki, Y. Kuwahara, H.Yamashita, Appl. Catal. A-Gen. 227 (2016) 45-52.

[12] H. Yin, Y. Kuwahara, K. Mori, H. Yamashita, J. Mater. Chem. A. 6 (2018) 10932–10938.

[13] M. Navlani-García, P. Verma, Y. Kuwahara, T. Kamegawa, K. Mori, H. Yamashita, J. Photochem. Photobiol. A Chem. 358 (2018) 327–333..

[14] S. Jo, P. Verma, Y. Kuwahara, K. Mori, W. Choi, H. Yamashita, J. Mater. Chem. A. 5 (2017) 21883–21892.

[15] M. Chandra, Q. Xu, J. Power Sources. 168 (2007) 135–142.

[16] J. García-Aguilar, M. Navlani-García, Á. Berenguer-Murcia, K. Mori, Y. Kuwahara, H. Yamashita, D. Cazorla-Amorós, RSC Adv. 6 (2016) 91768–91772.

[17] K. Mori, K. Miyawaki, H. Yamashita, ACS Catal. 6 (2016) 3128–3135.

[18] D. Salinas-Torres, M. Navlani-García, Y. Kuwahara, K. Mori, H. Yamashita, Catal. Today. (2019) 1-6

[19] M. Wen, Y. Cui, Y. Kuwahara, K. Mori, H. Yamashita, ACS Appl. Mater. Interfaces. 8 (2016) 21278–21284.

[20] J. Li, Q.L. Zhu, Q. Xu, Catal. Sci. Technol. 5 (2015) 525–530.

[21] A. Yousef, R.M. Brooks, M.M. El-Halwany, M.H. El-Newehy, S.S. Al-Deyab, N.A.M. Barakat, Ceram. Int. 42 (2016) 1507–1512.

[22] M. Zahmakiran, F. Durap, S. Özkar, Int. J. Hydrogen Energy. 35 (2010) 187–197.

[23] S.B. Kalidindi, U. Sanyal, B.R. Jagirdar, Phys. Chem. Chem. Phys. 10 (2008) 5870–5874.

[24] Y.W. Yang, Z.H. Lu, X.S. Chen, Mater. Technol. 30 (2015) 89–93.

[25] R. Leary, A. Westwood, Carbon. 49 (2011) 741–772.

[26] M.A. Andrade, R.J. Carmona, A.S. Mestre, J. Matos, A.P. Carvalho, C.O. Ania, Carbon. 76 (2014) 183–192.

[27] K. Woan, G. Pyrgiotakis, W. Sigmund, Adv. Mater. 21 (2009) 2233–2239.

[28] W. Wang, P. Serp, P. Kalck, C.G. Silva, J.L. Faria, Mater. Res. Bull. 43 (2008) 958–967.

[29] L. Bazli, M. Siavashi, A. Shiravi, Journal of Composites and Compounds. 1 (2019) 1.

[30] P. Vincent, A. Brioude, C. Journet, S. Rabaste, S.T. Purcell, J. Le Brusq, J.C. Plenet, J. Non. Cryst. Solids. 311 (2002) 130-137.

[31] H. Wang S. Dong Y. Chang J.L. Faria, J. Hazard. Mater. 236 (2012) 230-236.

[32] B. Xue, P. Chen, Q. Hong, J. Y. Lin, K.L. Tan, J. Mater. Chem. 11 (2001) 2378-2381.

[33] W. Zhang, G. Li, H. Liu, J. Chen, S. Ma, T. An, Environ. Sci.: Nano, 6 (2019) 948-958.

[34] J. Kong, Y-H. Qin, T-L.Wang, C-W. Wang, Int. J. Hydrogen Energy. 45 (2020) 1991-1997.

[35] A. Nourbakhsh S. Abbaspour, M. Masood, S. N. Mirsattari, A. Vahedi, K.J.D. Mackenzie, Ceram. Int. 42 (2016) 11901-11906.

[36] V. Dassireddy, B. Likozar, J. Taiwan Inst. Chem. E. 82 (2018) 331-341.

[37] A. Shafei, S. Sheibani, Mater. Res. 111 (2019) 198-206.

[38] J. Fernández-Catalá, L. Cano-Casanova, M.Á. Lillo-Ródenas, Á. Berenguer-Murcia, D. Cazorla-Amorós, Molecules. 22 (2017) 2243.

[39] A.K. Chatterjee, R.K. Sarkar, A.P. Chattopadhyay, P. Aich, R. Chakraborty, T. Basu, Nanotechnology. 23 (2012) 1-11.

[40] M.C. Biesinger, Surf. Interface Anal. 49 (2017) 1325–1334.

[41] Z. Zhang, P. Wang, J. Mater. Chem. 22 (2012) 2456-2464.

[42] D. Wang, X. Pan, G. Wang, Z. Yi, RSC Adv. 5 (2015) 22038–22043.

[43] N.O. Ramoraswi, P.G. Ndungu, Nanoscale Res. Lett. 10 (2015) 427.

[44] A. Saha, A. Moya, A. Kahnt, D. Iglesias,S. Marchesan, R. Wannemacher, M. Prato, J.J. Vilatela, D.M. Guldi, Nanoscale. 9 (2017) 7911-7921.

[45] C. C. Mercado, F. J. Knorr, J. L. McHale, S. M. Usmani, A. S. Ichimura and L. V. Saraf, J. Phys. Chem. C. 116 (2012) 10796–10804.

[46] M. Shaban, A.M. Ashraf, M.R Abukhadra, Sci. Rep. 8 (2018) 781.

[47] T.S. Natarajan, J.Y. Lee, H.C. Bajaj, W.K. Jo, R.J. Tayade, Catal. Today. 282 (2017) 13-23.

[48] Q. Zhou, H.Yang ,C. Xu, Int. J. Hydrogen Energy.41 (2016) 127174-12721.

[49] Q. Zhou, C. Xu, J. Colloid Interface Sci. 496 (2017) 235-242.